A Model-Based Approach for Automated Feature Extraction in Fundus Images

Huiqi Li
School of Computing
National University of Singapore
dcslihq@nus.edu.sg

Opas Chutatape
School of Electrical and Electronic Engineering
Nanyang Technological University
eopas@ntu.edu.sg

Abstract

A new approach to automatically extract the main features in color fundus images are proposed in this paper. Optic disk is localized by the principal component analysis (PCA) and its shape is detected by a modified active shape model (ASM). Exudates are extracted by the combined region growing and edge detection. A fundus coordinate system is further set up based on the fovea localization to provide a better description of the features in fundus images. The success rates achieved are 99%, 94%, and 100% for disk localization, disk boundary detection, and fovea localization respectively. The sensitivity and specificity for exudate detection are 100% and 71%. The success of the proposed algorithms can be attributed to the utilization of the model-based methods.

1. Introduction

The color fundus images are used to keep track of the eye diseases by ophthalmologists. Developing automatic fundus image analyzing and diagnosing system has been the ultimate aim of our research to facilitate clinical diagnosis. Extraction of the normal and abnormal features in color fundus images is fundamental and useful to automatic understanding of fundus images. The normal features of fundus images include optic disk, fovea and blood vessels. Exudates and hemorrhages are the main abnormal features for diabetic retinopathy, which is the leading cause of blindness in the working age population.

Optic disk is the brightest part in the normal fundus images, which can be seen as a pale, round or vertically slightly oval disk [1]. In [2] [3], the brightest pixels were clustered and the optic disk was located by the centroid of the largest cluster. In [4], disk was identified by the area with the highest variation in intensity of adjacent pixels. These bottom-up methods work well in normal fundus images, but they will lead to wrong disk localization when there are large areas of bright lesions similar to optic disk. The geometrical relationship between optic disk and blood vessels was utilized in the identification of optic disk in [5] [6], which are top-down methods. The idea sounds reasonable, but it is difficult to put into practice because vessel detection is a more complicated task.

The change in the shape, color or depth of optic disk is an indicator of various ophthalmic pathologies especially for glaucoma. The contour of optic disk was estimated as a circle or an ellipse in [2] [3] [7]. As the obtained circle or ellipse will not exactly match the disk boundary, the exact contour of optic disk has been investigated. 'Snakes' was proposed to detect the boundary of optic disk in [8] [9] [10] due to its ability to bridge discontinuities of the edges. The requirement of the manual initialization makes it semi-automatic. The main difficulty of these 'snakes' methods is how to remove the influence of vessels.

Exudates are one of the most common occurring lesions in diabetic retinopathy. The shape, brightness and location of exudates vary a lot among different patients. Techniques in the exudate detection can be classified into three categories: thresholding [3] [11] [12], edge detection [6] [13], and classification [14] [15]. The thresholding method is straightforward, but the automatic selection of the threshold is difficult. The main concern of the methods based on edge detection is how to distinguish the edges of exudates from the edges of vessels and other lesions. Statistical classification [15] and neural network [14] were also attempted, which are cataloged into the classification approach. It is still difficult for these methods to detect exudates robustly in fundus images.

Novel methods to detect optic disk, fovea, exudates, and to set up the fundus coordinate system are proposed in this paper. Model-based approaches are employed in the feature extraction, and the corresponding experiments are carried out to test the algorithms.

2. Methodology

2.1. Disk localization by PCA

Proceedings of the Ninth IEEE International Conference on Computer Vision (ICCV 2003) 2-Volume Set
0-7695-1950-4/03 $17.00 © 2003 IEEE

Principal component analysis (PCA) [16] [17], which belongs to the top-down strategies, is proposed to localize optic disk in this paper. The localization procedure is performed on the intensity image. There are two steps in the localization: the candidate regions are determined first and PCA is employed only to the candidate regions to speed up the whole processing.

The pixels with the highest 1% gray levels in intensity image are selected, which are mainly from the areas in optic disk or bright lesions. The single pass method [18] is employed to cluster these pixels. A cluster is abandoned if the number of the pixels in it is less than 0.04% of the total pixel number of the whole image, because it is most likely caused by noise or small bright lesions. A square candidate region, which is centered on the cluster's centroid and with the side of 1.4 times the average disk diameter, is defined for each remaining cluster.

In the PCA approach, disk space is obtained from the training images first. An input image is then projected on the disk space and its distance from the disk space is calculated. A square sub-image around the optic disk is cropped manually to obtain a training image. Scale normalization is performed by resizing it to $N \times N$ pixels, where N is the average disk diameter. Intensity normalization is next carried out by rescaling the intensity to the range of 0~255 via a simple linear quantization. The PCA transform is performed on the training vectors, which are in N^2 dimensions. Ten sub-images are employed as the training set here and the first six eigenvectors corresponding to the largest six eigenvalues are selected. These six eigenvectors can represent 90% of the total variance in the training set. The subspace defined by these eigenvectors is referred to as disk space. For each pixel in the candidate regions in an input image, an $N \times N$ sub-image with the pixel as the center is obtained automatically. The intensity normalization is carried out before the sub-image is projected onto the disk space by the PCA transformation. The distance from disk space, which measures the likeliness of optic disk, is defined as the Euclidean distance between the sub-image and its reconstruction onto the disk space.

Since the size of optic disk varies among individuals, PCA with different scales (0.8~1.2) is applied. Thus an input sub-image is compared with the eigendisks at a number of scales. The pixel (L_x, L_y) with the minimum distance in all the candidate regions and among all the scales is located as the disk center. The approximate size of the disk in a testing image can be obtained as well.

2.2. Disk boundary detection by a modified ASM

Some parts of the disk boundary are not well defined and some parts are partly obscured by blood vessels in fundus images, which make the detection of disk shape complicated. A modified active shape model (ASM), which is a parametric deformable model, is proposed to detect the disk boundary in this paper. The ASM method [19] [20] is a searching procedure to fit the point distribution model (PDM) in a new image to find the modeled object.

A shape of optic disk is represented by the position of n (n = 48) landmark points (see Fig. 1). The eight training shapes are aligned by a transformation that includes translation, rotation and scaling. The alignment is performed by minimizing the Euclidean distance between the shapes using a routine least square approach. PCA is next performed on the aligned training shapes. A shape model can be represented by

$$x = \bar{x} + \Phi\, b \tag{1}$$

where $\bar{x}$ is the mean shape of the aligned training set, $b = (b_1, b_2, \mathrm{K}\ , b_t)^T$ is termed shape parameter vector, and $\Phi = (\Phi_1, \Phi_2, \mathrm{K}\ , \Phi_t) \in R^{2n \times t}$ is the set of eigenvectors corresponding to the largest t eigenvalues of the covariance matrix of the training shapes. The first four eigenvectors are selected (t = 4) in our application. The model obtained in Eq. (1) is termed as PDM. It is a statistical description of the disk shape and its variations of the training set.

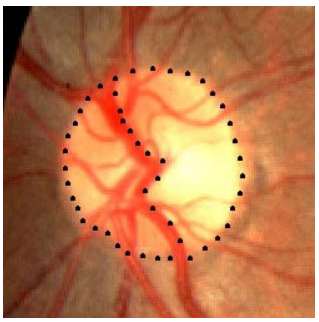

Figure 1. A shape instance

The space defined by the input image is referred to as image space and the space described by Eq. (1) is termed as shape space. The variables in the shape space and the image space are denoted by the lowercase and uppercase respectively in this paper. The transformation between the two spaces is defined by

$$X = T(x) = \begin{pmatrix} s\cos\theta & -s\sin\theta \\ s\sin\theta & s\cos\theta \end{pmatrix} \begin{pmatrix} x_i \\ y_i \end{pmatrix} + \begin{pmatrix} t_x \\ t_y \end{pmatrix} \tag{2}$$

where x and X are the shape models in the shape space and image space respectively. x_i, y_i denote the coordinates of the ith landmark point in the shape space. t_x, t_y represent the position of the model center in the

image space. $\tau(s,\theta,t_x,t_y)$ determines the transformation between the two spaces, which is termed as pose parameter.

The first step in ASM is initialization. The disk localization (L_x, L_y) and the mean shape are utilized to initialize the shape model in the image space according to Eq. (2), where $x = \bar{x},\ s = 1, \theta = 0,\ t_x = L_x,\ t_y = L_y$. Matching point detection is the second task. The first derivative of the intensity distribution along the normal profile is employed to find the matching point for each landmark point. A blood vessel is identified by a negative pulse followed by a positive pulse within the width range of vessels, and there is a single negative pulse where disk edge appears. The last part of ASM is parameter update. The pose parameter $\tau(s,\theta,t_x,t_y)$ can be updated by minimizing the following expression,

$$E_\tau = (Y - T(x))^T (Y - T(x)) \tag{3}$$

where Y is the set of matching points in the image space. The inverse transformation is used to transform the matching points Y in the image space back to y in the shape space. The shape parameter b is updated by projecting the matching points y onto the shape space.

$$b = \Phi^T (y - \bar{x}) \tag{4}$$

The constriction of $|b_i| \le 3\sqrt{\lambda_i}$ is applied to b_i so that a new shape will be similar to those in the training set, where λ_i is the ith largest eigenvalue. Finally the shape model is updated in the shape space and in the image space according to Eq. (1) and Eq. (2) respectively. The procedure of matching point detection and parameter update is iterated until the shape model X is converged.

The original ASM is improved in two aspects to eliminate the influence of the misplaced matching points: adding the self-adjusting weight and exclusion of the outlying points. These two modifications make the algorithm more favorable for the cases of weak edges. Weight factor is added to Eq. (3),

$$E_\tau = \sum_{i=1}^{n} (Y_i - X_i)^T W_i (Y_i - X_i) \tag{5}$$

where Y_i and X_i are the positions of the ith matching point and the ith model point in the image space respectively, and W_i is the weight factor. The transform for alignment is performed twice in each iteration: once with the initialized weight W_i and once with the adjusted W_i. The initialization of W_i is expressed as the following.

$$W_i = \begin{cases} 1 & Y_i \text{ is detected directly} \\ 0.7 & Y_i \text{ is estimated by nearby matching points} \\ 0 & Y_i \text{ is updated by } X_i \end{cases} \tag{6}$$

W_i is set to zero to eliminate the effect of Y_i when Y_i cannot be detected and the nearby matching points cannot be detected either. W_i is adjusted as the following, which is a negative feedback.

$$W_i = \begin{cases} 1 & E_i < 5 \\ 5/E_i & 5 \le E_i \le 15 \\ 1/E_i & E_i > 15 \end{cases} \tag{7}$$

where E_i is the Euclidean distance between the matching point Y_i and the updated landmark points X_i. The pose parameter τ in the iteration is finally obtained by minimizing Eq. (5) with the adjusted weight factor.

Another modification is excluding outlying points in the update of the shape parameter b. In each iteration, the shape parameter b is obtained in the same way as the original ASM first. A matching point is considered to be an outlying point or misplaced matching point when E_i between the matching point Y_i and the updated landmark point X_i is larger than a constant value. Those outlying points will not be used in obtaining shape parameter b,

$$b = \tilde{\Phi}^T (\tilde{y} - \tilde{\bar{x}}) \tag{8}$$

where n_m is the number of the outlying points, $b \in R^t$, $\tilde{\Phi} \in R^{2(n-n_m)\times t}$, $\tilde{y} \in R^{2(n-n_m)}$, $\tilde{\bar{x}} \in R^{2(n-n_m)}$. $\tilde{y}$, $\tilde{\Phi}, \tilde{\bar{x}}$ correspond to y, Φ and $\bar{x}$ in Eq. (4). The final shape model is estimated from Eq. (1) by reconstructing the shape model in $2n$-D space with the same parameter b obtained from Eq. (8).

2.3. Foveal coordinate system establishment

The locations of lesions are as important as their size and number to ophthalmologists [21]. A polar fundus coordinate system is established based on the fovea localization to describe the spatial locations of the features in fundus images. The fovea is the darkest part in most fundus images, while it is not obvious in some images due to high illumination or being covered by the lesions. It is situated about 2DD (DD = disk diameter) temporal to the optic disk in fundus images [1].

The main courses of blood vessels are extracted by the modified ASM introduced in section 2.2. They are represented by thirty landmark points (see Fig. 4(a)). Eight landmark sets are utilized to derive PDM and the first four eigenvectors are chosen. Observing the main courses of blood vessels, its shape is roughly a parabolic curve. The extraction result is fitted to a parabola for the future localization of fovea. A generalized parabola can be described as:

$$[(x - x_c)\sin\theta + (y - y_c)\cos\theta]^2 = 2p[(x - x_c)\cos\theta - (y - y_c)\sin\theta] \tag{9}$$

where $p/2$ is the focal length, (x_c, y_c) is the vertex, and θ is the rotation of the directrix. Four parameters (p, x_c, y_c, θ) need to be estimated. The ideas of Hough transform and linear least square fitting are combined in the curve fitting. The rotation θ is quantized to eliminate the nonlinear relationship between parameters. The vertex can be approximated at half optic disk radius nasal to optic disk, thus the parabolic fitting is simplified as estimating the only variable p by the least square fitting.

The candidate region of fovea is defined as a circle area. Its center is located at 2DD from the disk center along the main axis of the fitted parabola and its radius is set as 1DD. The pixels with the lowest intensity in the candidate region are selected, the sum of which is the area of optic disk, because the fovea is about the same size as optic disk [1]. These pixels are clustered by the single pass method [18]. The mean intensity of each cluster is calculated and the lowest two are compared. As the fovea is not obvious in some images, the comparison is to avoid mistaking the peripheral area, where the illumination is relatively dark, as fovea. When the difference is obvious and the number of pixels in the cluster is greater than 1/6 disk area, the foveal center is located by the centroid of the cluster with the lowest mean intensity, otherwise it is estimated at the center of the candidate region.

A polar coordinate system centered on the fovea is selected in our work according to the ETDRS report [21]. A fundus image is divided into 10 sub-fields by three fovea-centered circles with the radii of $1/3$ DD, 1DD, and 2DD respectively. The 10 sub-fields are defined as: (1) central sub-field within the inner circle; (2) four inner sub-fields between the inner and middle circles; (3) four outer sub-fields between the middle and outer circles; (4) far temporal sub-field temporal to the outer circle.

2.4. Exudate detection

Luv is selected as the suitable color space for exudate detection [22]. As the illumination in fundus images is not homogeneous, a fundus image is divided into sixty-four sub-images. Exudate detection is performed in each sub-image. The color difference of an object can be defined as:

$$D(i,j) = \sqrt{(L(i,j) - L_r)^2 + (u(i,j) - u_r)^2} \qquad (10)$$

where $L(i,j)$ and $u(i,j)$ are the colors of pixel (i,j) in the component L and u respectively. L_r and u_r are the reference colors of the object. The reference color is determined as the gravity center of the object [22]. Mean squared Wiener filter is performed to remove noise. A combined method of region growing and edge detection, which includes seed selection, edge detection and growing criteria, is employed here to detect the exudates. It is noted that some local minima are from the retinal background since the retinal background is uneven. Local minima below a certain threshold are chosen as the seeds. The edges in a sub-image are detected by the Canny edge detector. As some weak edges still cannot be detected, other features are examined besides checking if the region has reached an edge. Three criteria are employed:

(a) The gradient of the pixel is lower than a threshold T_1;

(b) The difference between the pixel value and the mean value of the region is lower than a threshold T_2;

(c) The difference between the pixel value and the value of the seed is lower than a threshold T_3.

3. Results and discussion

Eighty-nine color fundus images were obtained. Thirty-five images were provided by the Singapore National Eye Center (SNEC). Thirty are from another hospital. Another eighteen were captured by us, and the other six were downloaded from the Internet. All the images were resized to 512×512 pixels and saved as 24-bit Bitmap.

An example of the processing result is illustrated in Fig. 2. The disc localization algorithm was tested by all the eighty-nine images. The thirty-five images from SNEC were used as the testing images for the other proposed algorithms, as verification from ophthalmologists is only available for this batch of images. The success rates achieved are 99%, 94%, and 100% for disk localization, disk boundary detection, and fovea localization respectively. The sensitivity and specificity for exudate detection are 100% and 71% correspondingly. The details of the result are explained as the followings.

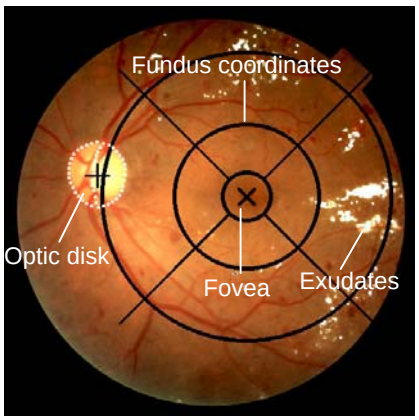

Figure 2. An example of processing result

3.1. Disk localization

Even though the ten training images are all obtained from the images provided by SNEC, satisfactory results could be achieved when the testing image are from other sources. The proposed algorithm failed in only one of the testing images, because there is a large area of lesions around the optic disk in that image and there is no such case in the training set. More constraints such as checking the convergence of the blood vessel network could be added to validate the localization of optic disk. The success rate of optic disk locating process is thus 99% based on the eighty-nine images tested.

3.2. Disk boundary detection

The accuracy of the obtained shape is evaluated by comparison with a reference shape labeled manually. Mean absolute distance (MAD) [23] is chosen here to indicate the difference of the two shapes. An example is shown in Fig. 3. The boundaries obtained by the original ASM and the modified ASM are represented by the dots in the figure. It can be seen that the boundary at the upper part cannot be detected correctly by the original ASM. However, the modified ASM could obtain a more suitable result. Thirty-five images were tested. The modified ASM detected the disk boundary successfully in thirty-three images, while the original ASM failed in seven of them. In the twenty-six images where both methods succeeded, the modified ASM also achieved better or at least as good as the results of ASM. The modified ASM needs less iterations in all the images except two cases. The comparison shows that the modified ASM can give more robust result than the original ASM especially when there are several misplaced matching points and also converges faster.

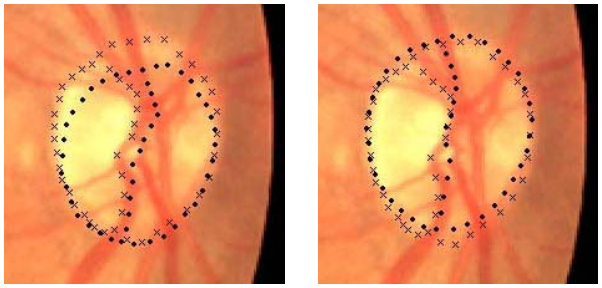

(a) Result by ASM (b) Result by the modified ASM

Figure 3. Boundary detected by the ASM and the modified ASM. 'x' indicates the reference shape.

3.3. Foveal coordinate system establishment

Fig. 4 shows an example of the detected vessel courses and the parabola fitting result. The fovea is detected directly by the centroid of the darkest cluster in twenty-one of the testing images. It is estimated in the other fourteen images. The localization of the fovea is within the region of fovea in all these thirty-five images. But the localization deviates slightly from the apparent center in three of the images when evaluated by the human eyes. The localization of fovea is estimated in all of these three images. The reason of the deviation is that the estimation may not be precise.

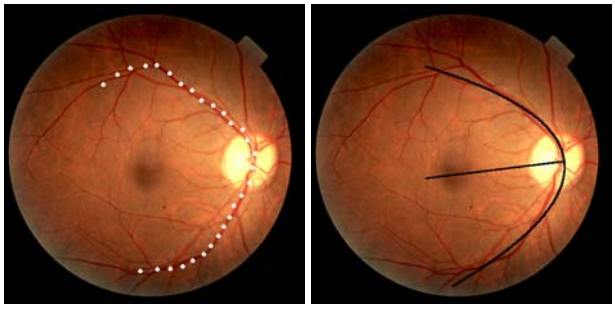

(a) Result of vessel extraction (b) Result of parabola fitting

Figure 4. The detected vessel and parabola fitting

3.4. Exudate detection

In the thirty-five testing images, seven images were identified to have no exudate by ophthalmologists. The presence of exudates was successfully detected in all the twenty-eight images. However, exudates were detected by our algorithm in two images in which no exudate is present. The sensitivity and specificity is 100% and 71% respectively. Fig. 5 shows two examples of exudate detection. The detected exudates are represented by the white color in the figure, where foveal fundus coordinates are overlaid. Though the total number and area of exudates in Fig. 5(a) are both larger than the exudates in Fig. 5(b), the exudates in Fig. 5(b) have more harm to the vision than those in Fig. 5(a). The exudates within the inner circle will affect the vision of patients more than the exudates in other locations. This conclusion has been verified by the ophthalmologists. Thus the distribution of exudates needs to be analyzed to indicate the severity of the retinal diseases.

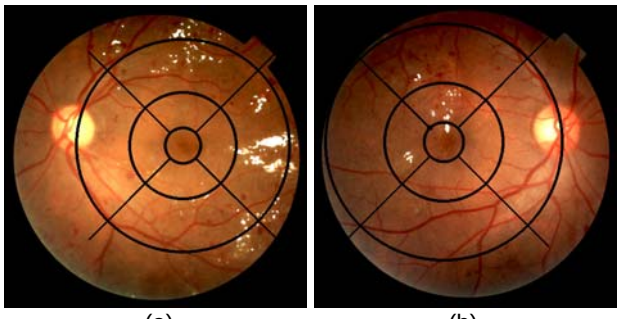

(a) (b)

Figure 5. Examples of exudate detection

4. Conclusion

The algorithms to extract features automatically and robustly in color fundus images were proposed in this paper. PCA is employed to locate optic disk; A modified ASM is proposed in the shape detection of optic disk; A fundus coordinate system is established based on the fovea localization; An approach to detect exudates by the combined region growing and edge detection is proposed. The success rates of disk localization, disk boundary detection, and fovea localization are 99%, 94%, and 100% respectively. The sensitivity and specificity of the exudate detection are 100% and 71% correspondingly. The success of the proposed algorithms can be attributed to the utilization of the model-based methods. The satisfactory feature detection could make the automatic analyzing system become more reliable. The generalization of the models could be improved when larger data source is available. Further tests should be carried out on the proposed algorithms to make them ultimately acceptable for clinical purposes.

5. References

[1] H. W. Larsen, *The Ocular Fundus: a Color Atlas*, Munksgaard, Copenhagen, 1976, pp. 10-12.

[2] S. Tamura, Y. Okamoto and K. Yanashima, "Zero-crossing interval correction in tracking eye-fundus blood vessels", *Pattern Recognition*, Vol. 21, No. 3, 1988, pp. 227-233.

[3] Z. Liu, O. Chutatape and S. M. Krishnan, "Automatic image analysis of fundus photograph", *Proceedings of the International Conference of the IEEE Engineering in Medicine and Biology Society*, Vol. 2, 1997, pp. 524-525.

[4] C. Sinthanayothin, J. F. Boyce, H. L. Cook and T. H. Williamson, "Automated location of the optic disk, fovea, and retinal blood vessels from digital colour fundus images", *British Journal of Ophthalmology*, Vol. 83, No. 8, 1999, pp. 902-910.

[5] G. Zahlmann, B. Kochner, I. Ugi, D. Schuhmann, B. Liesenfeld, A. Wegner, M. Obermaier and M. Mertz, "Hybrid fuzzy image processing for situation assessment", *IEEE Engineering in Medicine and Biology*, 2000, pp. 76-83.

[6] K. Akita and H. Kuga, "A computer method of understanding ocular fundus images", *Pattern Recognition*, Vol. 15, No. 6, 1982, pp. 431-443.

[7] M. Lalonde, M. Beaulieu and L. Gagnon, "Fast and robust optic disk detection using pyramidal decomposition and Hausdorff-based template matching", *IEEE Transactions on Medical Imaging*, Vol. 20, No. 11, 2001, pp. 1193-1200.

[8] S. Lee and L. M. Brady, "Integrating stereo and photometric stereo to monitor the development of glaucoma", *Proceedings of the British Machine Vision Conference*, 1990, pp. 193-198.

[9] D. T. Morris and C. Donnison, "Identifying the neuroretinal rim boundary using dynamic contours", *Image and Vision Computing*, Vol. 17, 1999, pp. 169-174.

[10] F. Mendels, C. Heneghan and J. P. Thiran, "Identification of the optic disk boundary in retinal images using active contours", *Proceedings of the Irish Machine Vision and Image Processing Conference*, 1999, pp. 103-115.

[11] N. P. Ward, S. Tomlinson and C. J. Taylor, "Image analysis of fundus photographs. The detection and measurement of exudates associated with diabetic retinopathy", *Ophthalmology*, Vol. 96, 1989, pp. 80-86.

[12] R. Phillips, J. Forrester, P. Sharp, "Automated detection and quantification of retinal exudates", *Graefe's Archive for Clinical and Experimental Ophthalmology*, Vol. 231, 1993, pp. 90-94.

[13] H. Li and O. Chutatape, "Fundus image features extraction," *Proceedings of the 22nd Annual International Conference of the IEEE Engineering in Medicine and Biology Society*, Vol. 4, 2000, pp.3071 -3073.

[14] G. G. Gardner, D. Keating, T. H. Williamson, and A. T. Elliott, "Automatic detection of diabetic retinopathy using an artificial neural network: A screening tool", *British Journal of Ophthalmology*, Vol. 80, No. 11, 1996, pp. 940-944.

[15] H. Wang, W. Hsu, K. G. Goh, and M. L. Lee, "An effective approach to detect lesions in color retinal images", *Proceedings of IEEE Computer Society Conference on Computer Vision and Pattern Recognition*, 2000, pp. 181-187.

[16] M. Turk and A. Pentland, "Eigenfaces for recognition", *Journal of Cognitive Neuroscience*, Vol. 3, No. 1, 1991, pp. 70-86.

[17] H. Li, O. Chutatape, "Automatic detection and boundary estimation of the optic disk in retinal images using a model-based approach", *Journal of Electronic Imaging*, Vol. 12, No. 1, 2003, pp.97-105.

[18] D. R. Hill, "A vector clustering technique", *Mechanized Information Storage, Retrieval and Dissemination*, North-Holland, Amsterdam, 1968.

[19] T. F. Cootes, C. J. Taylor, D. H. Cooper and J. Graham, "Active shape models-Their training and application", *Computer Vision and Image Understanding*, vol. 61, No. 1, 1995, pp.38-59.

[20] H. Li, O. Chutatape, "Boundary detection of optic disk by a modified ASM method", *Pattern Recognition*, Vol. 36, No. 9, 2003, pp. 2093-2104.

[21] ETDRS Report Number 10, "Grading diabetic retinopathy from stereoscopic color fundus photographs - An extension of the modified Airlie house classification", *Ophthalmology*, Vol. 98, 1991, pp. 786-806.

[22] G. Luo, O. Chutatape, H. Li and S. M. Krishnan, "Abnormality detection in automated mass screening system of diabetic retinopathy", *Proceedings of 14th IEEE Symposium on Computer-Based Medical Systems*, 2001, pp. 132 –137.

[23] V. Chalana, D. T. Linker, D. R. Haynor and Y. Kim, "A multiple active contour model for cardiac boundary detection on echocardiographic sequences", *IEEE Transactions on Medical Imaging*, Vol. 15, No. 3, 1996, pp.290-298.